Equilibrium or Quenched: Fundamental Differences between Lipid Monolayers, Supported Bilayers, and Membranes

Erik B. Watkins,[†,‡,*] Chad E. Miller,[§] Wei-Po Liao,[⊥] and Tonya L. Kuhl[†,⊥,∥,*]

[†]Biophysics Graduate Group, University of California, Davis, California 95616, United States, [‡]Institut Laue-Langevin, BP 156, 38042 Grenoble, France, [§]Stanford Synchrotron Radiation Lightsource, Menlo Park, California 94025, United States, [⊥]Department of Chemical Engineering and Materials Science, University of California, Davis, California 95616, United States, and [∥]Department of Biomedical Engineering, University of California, Davis, California 95616, United States

ABSTRACT In this work, we establish fundamental differences between the structure and packing of lipids in monolayers, supported bilayers, and multilayer films. High resolution grazing incidence X-ray diffraction reveals that monolayer structure is largely retained upon deposition onto substrates with the area per molecule controlled by deposition pressure. Such structural changes are consistent with a quenched rather than equilibrated supported membrane structure. Supported bilayers formed by vesicle fusion exhibit structural similarity to bilayers deposited at 38 mN/m, whereas packing in lipid multilayers more closely resembled bilayers deposited below 30 mN/m. At the molecular level, coupling between opposing lipid acyl chains is observed for all deposition pressures with the outer leaflet templating on the inner leaflet. Leaflet coupling induces a small condensation in the area per lipid molecule and a surprising increase in acyl chain tilt. Moreover, supported lipid bilayers exhibit preferential acyl chain alignment: the system cannot be modeled with freely rotating acyl chains as in free-standing lipid monolayers. Such acyl chain alignment is consistent with orientational texture of lipid tilt directors at larger length scales. These findings clearly demonstrate that supported, gel-phase bilayer membrane structure can be controlled and maintained by deposition onto solid supports and that increasing surface pressure induces preferential alignment of the acyl chains both within and between membrane leaflets.

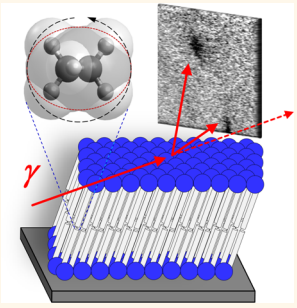

KEYWORDS: biomembrane · Langmuir–Blodgett · DPPC · X-ray grazing incidence diffraction · phospholipid · supported lipid membrane · lipid bilayer

Substrate supported lipid bilayers are routinely used as model biomembranes for fundamental studies, as well as in biosensing applications.[1−3] Over the past decade alone, more than 5000 articles are returned for a search of "supported lipid membrane".[4] The reasons for this activity include the number of surface sensitive techniques that can be applied to such systems, the ease in changing solution conditions or experimental parameters, and the capability to couple the supported membrane to a physicochemical transducer in the engineering of biosensors. It has been shown that the structure and fluidity of supported lipid bilayers is similar to those of free-standing membranes.[5] Less well understood is how lipid properties and self-organized structures differ between monolayers, multilayer lipid films, and supported bilayers and how molecular scale ordering of lipids within supported bilayers can be manipulated.[6]

X-ray and neutron scattering methods have been widely used to characterize lipid membrane structure in a variety of architectures and have provided atomic scale resolution of membrane thickness, density distribution of the molecular moieties, and membrane fluctuations.[7−12] Two significant advantages of neutron scattering measurements are the ability to penetrate materials to study buried interfaces and to change contrast and highlight specific features of the membrane through isotopic labeling. On the other hand, the flux of X-ray synchrotrons far exceeds neutron sources allowing much higher resolution measurements and enabling the use of techniques that have an inherently lower scattering

* Address correspondence to erik.b.watkins@gmail.com, tlkuhl@ucdavis.edu.

Received for review October 11, 2013 and accepted March 6, 2014.

Published online March 06, 2014
10.1021/nn4052953

signal. Recently, the combination and corefinement of X-ray and neutron scattering from multilayer systems has been used to accurately determine one of the most fundamental properties of lipids in membranes: the area per lipid molecule.[13] Performing experiments on multilamellear lipid structures (either unoriented phases or oriented multilayer stacks) has the advantages of strong scattering signals due to the larger quantities of material, as well as being ideally suited for the investigation of membrane−membrane interactions. Studied since the late 1960s, diffraction from these systems has provided the foundation of our understanding on lipid structure and packing.[14−16] However, the thin hydration layer between membranes in multilamellear lipid structures poses some limitations and may encumber studies involving interactions between membranes and water-soluble molecules. Additionally, multilayer stacks are not stable in bulk water and must be measured in humidified air, which in some cases may limit their relevance to native biological membranes or their use in devices. Other model membrane systems, such as single lipid monolayers and supported bilayers, can be investigated through the use of scattering techniques specifically tuned to enhance the signal from surface structures. For example, both X-ray and neutron reflectivity have been extensively used to characterize the structure of lipid monolayers at the air−water interface as a function of surface pressure, solution conditions, and the presence of proteins.[17] Further, high synchrotron X-ray fluxes facilitate grazing incidence X-ray diffraction (GIXD) measurements from single lipid monolayers in the solid or gel phase. This technique can be used to provide molecular scale details of in-plane lipid packing, unit cell dimensions, tilt, and coherence length (length scale over which the lipid layer diffracts) as well as out-of-plane coherence lengths.[18,19] However, since only half the membrane structure is approximated by lipid monolayers, they are not suitable model systems for studies involving interactions between lipid leaflets or transmembrane phenomena. While diffraction techniques have been widely employed to investigate lipid packing in monolayers and density distributions of the lipid moieties in multilamellar systems, their application to single, supported lipid bilayers has been relatively limited. This is in large part due to experimental difficulties in probing the buried membrane film at the liquid−substrate interface. As a result, lower resolution neutron reflectivity measurements have been the primary scattering tool to characterize the structure of single supported lipid membranes.[20,21] Following recent advancements in the application of high energy synchrotron radiation, X-ray reflectivity can now provide higher resolution out-of-plane structure than neutron reflectivity measurements.[22,23] Further, GIXD provides sub-Å resolution of the in-plane packing of solid or gel phase lipids in single supported bilayers: structural information about supported bilayers that cannot be obtained by any other technique.[24]

Remarkably, the packing of lipids in supported bilayers, especially as a function of deposition conditions, has not been extensively studied. Such high resolution structural information has the potential to shed light on the role of leaflet−leaflet interactions in lipid raft formation and stabilization as well as enabling the design of biosensors with specific functionality. In this work, we compare and contrast the structure of DPPC lipid monolayers at the air−water interface and supported bilayers at the solid−water interface using high resolution X-ray surface scattering measurements. We specifically address whether the in-plane structure of a substrate supported membrane can be controlled by deposition conditions and how the packing of molecules within lipid bilayers is inherently different from that of lipid monolayers due to interactions between bilayer leaflets and interactions between the substrate and the inner leaflet. Further, details of the DPPC packing in monolayer and bilayers, such as area per molecule (APM) and out-of-plane tilt of the lipids, are compared to the well established results obtained from multilayer diffraction in the literature.

RESULTS

The surface pressure isotherm (π-A) of DPPC and specific surface pressures studied in this work are shown in Figure 1. Figure 2A shows a representative GIXD contour plot of the scattered intensity as a function of q_{xy} and q_z for a DPPC bilayer deposited at a surface pressure of 30 mN/m. The image reveals two

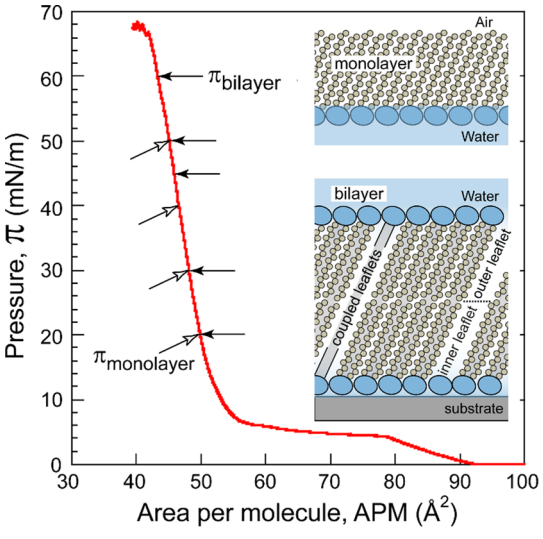

Figure 1. Room temperature (21 ± 2 °C) DPPC isotherm at the air−water interface. The open arrows show surface pressures of monolayer measurements (top schematic); the closed arrows show deposited pressures of LB−LS supported bilayers (bottom schematic). The bilayer schematic depicts molecular level coupling of the acyl chains between the two lipid leaflets.

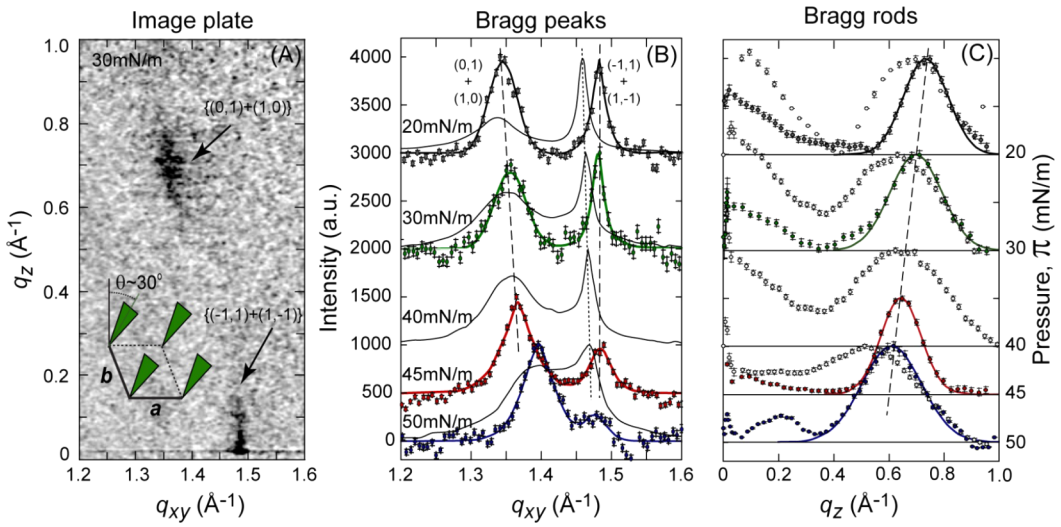

Figure 2. (A) Example image plate of GIXD from a single supported DPPC bilayer deposited at 30 mN/m. The projection of the quartz substrate is defined as $q_z = 0$ Å^{-1}. Bragg peaks (B) are the intensity resolved in the q_{xy}-direction and integrated over the relevant $q_z = 0$ Å^{-1} range. Bragg rods (C) are the intensity resolved in the q_z direction and integrated over the q_{xy} range. Two Bragg peaks were observed with Miller indices, $\{(0,1)+(1,0)\}$ and $\{(-1,1)+(1,-1)\}$ corresponding to a distorted hexagonal unit cell. (B) Bragg peaks from DPPC monolayers as a function of surface pressure (black lines) and supported bilayers as a function of deposition pressure (filled points). From top to bottom, data points corresponds to 20 (gray), 30 (green), 45 (red), and 50 mN/m (blue) bilayers. Monolayer Bragg peaks at 20, 30, 40 and 50 mN/m are shown for comparison. Colored lines are fits to the Bragg peaks using pseudo Voigt functions. Dashed lines are guides to indicate the shift in the peak position with increasing surface pressure. (C) Bragg rods from DPPC monolayers (open points) and bilayers (filled points). From top to bottom, data points corresponds to 20 (gray), 30 (green), 45 (red), and 50 mN/m (blue) bilayers. Monolayer Bragg rods at 20, 30, 40 and 50 mN/m are shown for comparison. Solid lines are Gaussian fits to the combined $\{(0,1)+(1,0)\}$ peaks from the bilayers.

peaks indicative of a distorted hexagonal lattice with the lipid acyl chains tilted toward their nearest neighbor (NN) as shown in the inset schematic. Figure 2B,C shows the diffraction data as a function of surface pressure for monolayers and of deposition pressure for bilayers. The plots are obtained by integrating the image plate over q_z to yield Bragg peaks and over q_{xy} to yield Bragg rods. Up to 45 mN/m the lower q_{xy} Bragg peak position shifts proportionally to the surface pressure (dashed lines). These shifts are consistent with an approximately linear decrease in APM and tighter packing of the lipids with increasing surface pressure. A break in this linear dependence occurs at 50 mN/m where the π-A isotherms show decrease in trough area over time when constant surface pressure is maintained, indicating that the DPPC monolayer begins to lose stability (data not shown).

To obtain unit cell parameters and an APM, the Bragg peak positions (Figure 2B) were indexed using a distorted hexagonal unit cell with NN tilt orientation. Symmetry is partially broken in this unit cell resulting in a distinct $\{(-1,1)+(1,-1)\}$ peak and a combined $\{(0,1)+(1,0)\}$ peak. Since the degeneracy of the (0,1) and (1,0) peaks was not broken, oblique unit cells were not considered when fitting the Bragg peaks. The two remaining first-order reflections $\{(-1,0)+(0,-1)\}$ are at negative q_z and because of attenuation by the underlying quartz or water were generally not measured. Integrating the area under each measured Bragg peak demonstrates that diffraction from monolayers obeys the multiplicity rule, which requires that the reflections have equal intensity: the area of the $\{(-1,1)+(1,-1)\}$ peak visible at positive q_z is approximately half that of the combined $\{(0,1)+(1,0)\}$ peak area. In contrast, for bilayers the relative intensity of the $\{(-1,1)+(1,-1)\}$ reflection is diminished and the mismatch between relative intensities becomes larger with higher deposited surface pressure. Violation of the multiplicity rule in supported membranes suggests that the diffraction originates from nonisotropically ordered lipid tails. In other words, the acyl chains in a membrane lack rotational symmetry around their long axis and cannot be described using a free rotator model.[25,26] As we describe below, coupling between the bilayer leaflets that comprise the membrane may contribute to the rotational hindrance of the acyl chains.

In general, the $\{(0,1)+(1,0)\}$ Bragg peak position shifts linearly as a function of surface pressure for both monolayers and bilayers. For equivalent surface pressures, however, the $\{(-1,1)+(1,-1)\}$ peak position of the bilayers are consistently shifted to higher q_{xy} relative to the monolayers demonstrating a small reduction in area per molecule (or condensation in packing) in a bilayer configuration. Fitting pseudo Voigt functions to the Bragg peaks enables unit cell parameters (a, b, γ) to be obtained, where $a = b$ when the acyl chains are tilted toward their nearest neighbor. The unit cell parameters from this modeling approach for both monolayers and bilayers are presented in Table 1. For freely rotating chains, the acyl chains are approximated as close packed

TABLE 1. Structural Packing Parameters of DPPC Monolayers and Bilayers Obtained from GIXD Analysis

	a [Å] ±0.005	γ [deg] ±0.1	APM [Å^2] ±0.05	θ_{BPK} [deg] ±0.1	A_{BPK} [Å^2] ±0.05	θ_{BR} [deg] ±0.1	A_{BR} [Å^2] ±0.05	L_C [Å] ±0.1
DPPC Bilayers								
20 mN/m	5.079	113.1	47.46	29.1	20.73	33.1	19.88	33.1
30 mN/m	5.065	113.8	46.94	27.7	20.78	31.5	20.01	28.3
Vesicle fusion	5.045	114.1	46.46	27.0	20.70	30.5	20.02	28.7
45 mN/m	5.035	114.4	46.18	26.4	20.68	29.1	20.18	36.8
50 mN/m	5.012	116.1	45.12	22.2	20.88	27.2	20.07	24.6
60 mN/m	5.094	114.2	47.36	26.8	21.14	31.9	20.10	27.1
DPPC Monolayers								
20 mN/m	5.128	114.3	47.96	26.8	21.40	31.0	20.55	17.5
30 mN/m	5.104	114.4	47.43	26.4	21.24	29.3	20.68	15.4
30 mN/m[a]	5.110	114.9	47.36	25.2	21.43	29.4	20.64	20.9
40 mN/m	5.085	114.8	46.97	25.7	21.16	28.6	20.62	16.2
50 mN/m	5.036	116.0	45.36	22.5	20.95	23.4	20.81	15.4

[a] Monolayer supported on quartz.

cylinders with an out-of-plane tilt (θ). This geometry forces a relationship between the unit cell parameter γ and tilt magnitude: $\theta = \cos^{-1}[\tan(\gamma/2)\cdot\tan(30)]$. With this approach, the tilt magnitudes were estimated directly from the Bragg peak positions and followed the same trend as values obtained by fitting the q_z intensity distribution of the Bragg rods described next.

Analysis of the Bragg rods (diffraction integrated over q_{xy}, Figure 2C) provides information on the orientation of the acyl chains out of the membrane plane (along the bilayer normal). In the monolayers, two maxima are observed: a $\{(-1,1)+(1,-1)\}$ low q_z maximum and the maximum corresponding to the combined $\{(0,1)+(1,0)\}$ reflection at high q_z. Half of the low q_z $\{(-1,1)+(1,-1)\}$ reflection cannot be observed due to water/substrate absorption. As previously described in the Bragg peak analysis, for bilayers the intensity of the $\{(-1,1)+(1,-1)\}$ reflection is significantly diminished relative to the combined $\{(0,1)+(1,0)\}$ reflection. The position of the combined $\{(0,1)+(1,0)\}$ reflection is proportional to the tilt magnitude θ for NN packing and shifts to smaller q_z with increasing surface or deposition pressure due to a decreasing tilt of the acyl chains (dashed line). Bragg rod maxima also indicate that the acyl chains are tilted slightly more in the bilayers compared to monolayers for a given surface pressure. Assuming that the lipid chains point toward their nearest neighbor in the unit cell, the tilt magnitude (θ) can be determined from the q_z position of the out of plane reflection ($q_z^{\{(0,1)+(1,0)\}}$) by:

$$\theta = \tan^{-1}\left(\frac{q_z^{\{(0,1)+(1,0)\}} a\cos\left(\frac{\gamma}{2}\right)}{\pi}\right)$$

where a and γ are unit cell parameters.[27] With the use of this equation and a Gaussian fit to obtain $q_z^{\{(0,1)+(1,0)\}}$, tilt magnitudes were extracted and are reported in Table 1. While the same trend in tilt magnitude was observed as in calculations based solely on Bragg peak positions, the values were consistently smaller by a mean of 2.7° for monolayers and of 4.1° for bilayers. Since the tilt values obtained from the Bragg rods are not explicitly dependent on a cylindrical molecular shape, these discrepancies cast further doubt on the assumption that the free rotator model can be applied, particularly in the bilayer case, to the packing of lipid acyl chains. However, it is not possible to rule out other perturbations to the cylindrical symmetry of the tails, such as constraints imposed by lipid headgroup packing, which could lead to the discrepancy in calculated tilts.

The full width half-maximum (fwhm) in q_z of the $\{(0,1)+(1,0)\}$ Bragg rod reflections can be used to estimate the corresponding real-space length of the scattering entity (here, acyl chains) from $L_c = 2\pi/\text{fwhm}$. The widths of the Bragg rod maxima for bilayers are approximately half as broad as in the monolayer case indicative of diffraction from acyl chains coupled across the bilayer leaflets. Specifically, the acyl chains of the opposing leaflets are in registry on a molecular scale across the bilayer and scatter as one entity as shown schematically in Figure 1. For all deposition pressures, Gaussian fits to the bilayer Bragg rods yield fwhm corresponding to real space lengths greater than a single acyl chain, unambiguously demonstrating coupling between bilayer leaflets. However, a significant decrease in the fwhm was measured in the 50 mN/m bilayer case indicating higher disorder. As reflectivity profiles demonstrate that the thickness of the bilayer is very similar regardless of deposition pressure, this suggests lipids are "over packed" at higher pressures presumably due to increasing steric repulsion between the head groups. Additionally, the 30 mN/m monolayer deposited at the solid-air interface exhibited a smaller fwhm than monolayers at the air−water interface indicating that a greater length of the hydrocarbon chain contributed to the diffraction signal.

Figure 3 compares the Bragg rod distribution of 30 mN/m DPPC monolayers at both the air−water and solid-air interfaces with a bilayer deposited at 30 mN/m, and a bilayer formed by vesicle fusion. As shown schematically in the inset, an all trans-configuration of CH_2 groups has an electron density, dominated by the carbon atoms, that is roughly elliptical when projected along the acyl chain backbone. The van der Waals (VDW) radius of carbon (1.70 Å) and the separation between carbons projected along the chain backbone (0.88 Å) were used to approximate the cross sectional electron distribution of the lipid tails as an ellipse with a major axis of 2.14 Å and a minor axis of 1.70 Å. In the free rotator model, this elliptical

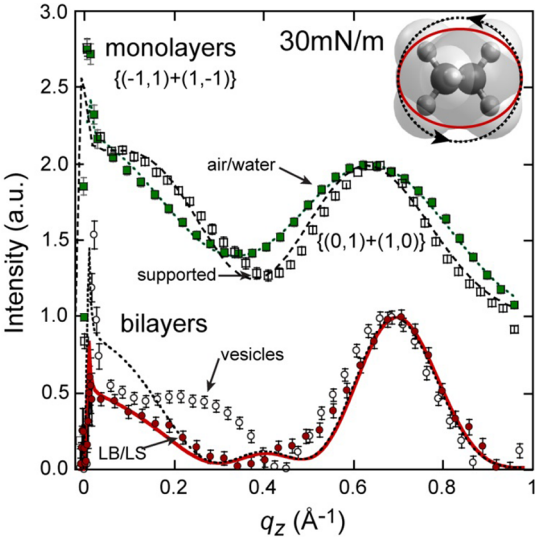

Figure 3. Bragg rods for a DPPC monolayer at the air−water interface at 30 mN/m surface pressure (top, green filled symbol) compared to a monolayer deposited on a quartz surface at 30 mN/m (top, open symbol), a bilayer deposited at 30 mN/m (bottom, red filled symbol), and a bilayer formed via vesicle fusion (bottom, open symbol). Monolayer data is offset vertically for clarity. Dotted lines are free rotator model fits calculated using cylindrically symmetric electron distributions arranged in unit cells obtained by fitting the corresponding Bragg peaks. The solid line is a fit using a $g = -0.7$ nonfree rotator model with tilt direction 5° from NN and a Gaussian distribution of acyl chain orientations centered at $\varphi = 90°$. With the exception of the rotational order of the chains, all other parameters in the bilayer fit matched the parameters of the free rotator model. The schematic inset represents the cylindrical cross section used for the free rotator model (dotted line) and the elliptical cross section used for the nonfree rotator model (solid line).

distribution was allowed to spin around the axis of the backbone resulting in a cylindrical electron distribution with a radius of 2.14 Å. Free rotator models (dotted lines) with nearest neighbor tilt, typically used to describe gel phase DPPC diffraction, fit the monolayer data at the air−water interface but failed to fit the bilayer data. The monolayer at the solid-air interface was also fit using a free rotator model with a small perturbation of the in-plane tilt direction to 9° from NN. Attempts to reproduce the bilayer diffraction using oblique unit cells and intermediate in-plane tilt directions were also unsuccessful. While these models were able to capture the high q_z features of the bilayer data, due to the multiplicity rule no free rotator model exists without equivalent intensity at low q_z. In a nonfree rotator model, the backbone orientations are restricted resulting in an electron density distribution that is not rotationally symmetric. Previously, calculations using a nonfree rotator model correlating the electron distribution to the position of nuclei along the hydrocarbon backbone were shown to alter the relative intensity of DPPC diffraction peaks.[28] However, the discrete positions of atoms do not fully capture the spatial distribution of a molecule's electron cloud. Here, the electron distribution of the hydrocarbon chain was approximated by a uniform electron density elliptical cylinder with cross section described above. Our approach was to use the simplest possible elliptical cylinder model corresponding to the hydrocarbon chain conformation and VDW radii. It should be noted that the calculated diffraction pattern depends on the ellipse dimensions so further optimization to better approximate the actual electron density distribution may yield more accurate descriptions of chain order. With this model, the distribution of chain orientations in the plane can be described by the rotational order parameter $g = \langle 2\cos^2\varphi - 1\rangle$ where φ is the angle between the major axis of the ellipse and the direction of tilt.[29] Following this definition, a given value of g may correspond to either a fixed orientation or a distribution of φ angles. To better approximate the measured data, nonfree rotator models were implemented using elliptical cylinders with a Gaussian distributions of φ centered at 90°. Under this constraint, the rotational order parameter ranges from $g = 0$ for a free rotator model to $g = -1$ for a fixed orientation with the major axes of the ellipse orthogonal to the tilt direction ($\varphi = 90°$). The best fit to the bilayer data (solid line) was obtained for a tilt direction 5° from NN and $g = -0.7$ corresponding to a Gaussian distribution of φ angles with a fwhm of 57° (more detail provided below and in Figure 4). The χ^2 metric was employed to evaluate the goodness of fit yielding $\chi^2 = 10.3$ for the $g = -0.7$ model compared to $\chi^2 = 13.1$ for a single fixed orientation and $\chi^2 = 24.6$ for a free rotator model. Both the free rotator and rotationally ordered models maintained the same parameters for the electron distribution and tilt magnitude, but when we partially restricted the rotational freedom of the molecules, an improved match to the measured data was achieved. Although the vesicle fusion data has features that are not reproduced by this simple model, the Bragg rod was also better approximated using a model in which the electron density of the acyl chains is rotationally asymmetric. Deviation from the model may be attributed to greater disorder and more variability of the lipid packing in the bilayer formed by vesicle fusion. We further comment that the nonfree rotator model used to describe lipid packing in bilayers is consistent with previously observed tilt texture in lipid monolayers and bilayers.[30−32]

Rotational ordering of the acyl chains in DPPC bilayers was also investigated as a function of deposition surface pressure. Figure 4 shows that between 20 and 45 mN/m the relative intensity of the low q_z Bragg rod maxima systematically decreased with increasing surface pressure. For all cases, the intensity distributions at low q_z could not be reproduced by a free rotator model. Instead, the Bragg rods show that the acyl chains become more ordered (less rotation disorder) with increasing deposition pressure. A series of rotational order parameters, g, were calculated to

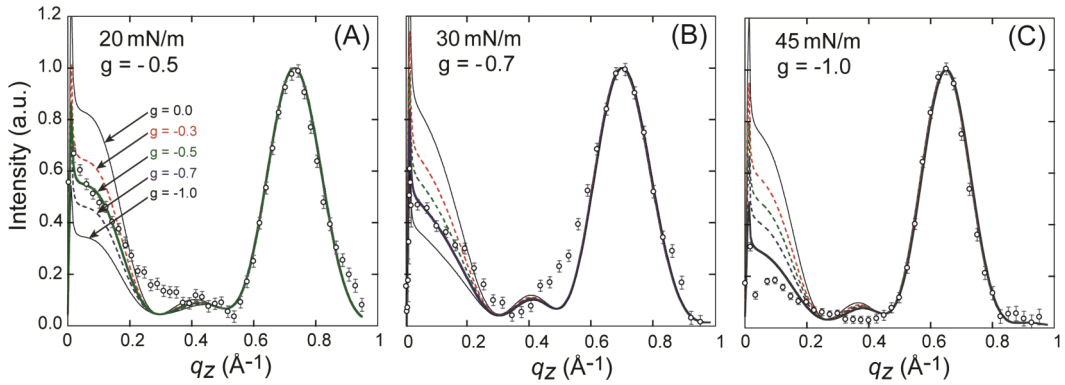

Figure 4. Nonfree rotator models for Bragg rod diffraction from DPPC bilayers at 20, 30, and 45 mN/m. Calculations for rotational ordering of the acyl changes ranging from g = 0.0 to g = −1.0 are compared to the data. Elliptical cylinders with major axis of 2.14 Å and a minor axis of 1.7 Å were used to approximate the electron density of the hydrocarbon chains and all calculations are for lipid arrangements with in-plane tilt direction 5° from NN and Gaussian distributions of chain backbone rotations centered at φ = 90°. The best fits to the data were obtained for a g = −0.5 distribution at 20 mN/m, g = −0.7 at 30 mN/m and g = −1.0 at 45 mN/m demonstrating a decrease in rotational freedom with increasing surface pressure.

simulate the data. All calculations employed the elliptical cylinder parameters used previously and an in-plane tilt direction 5° from NN. As described above, the best fit to the 30 mN/m data was obtained with a g = −0.7 Gaussian distribution of chain orientations. The 20 mN/m bilayer Bragg rod was best fit (χ^2 = 5.6) by a g = −0.5 Gaussian distribution of chain orientations with a fwhm of 80°. In contrast, a single fixed orientation model yielded χ^2 = 16.3 and a free rotator model χ^2 = 19.2. At 45 mN/m, there was the greatest deviation between the data and the diffraction calculated using a free rotator model (χ^2 = 66.5). The closest match was obtained for acyl chains with a fixed orientation orthogonal to the tilt direction (χ^2 = 4.2). Despite such a constrained molecular orientation, the model was incapable of completely reproducing the reduced intensity in the low q_z maximum. This may be attributed to limitations of the elliptical cylinder used to approximate the electron density along the hydrocarbon chain.

Finally for bilayers deposited at high surface pressures, asymmetry in the diffracted intensity at positive and negative q_{xy} was observed (Figure.5). This asymmetry emerged at 45 mN/m where diffraction was observed on both sides of the direct beam (positive and negative q_{xy}) but with unequal intensities. At 50 and 60 mN/m, where the Langmuir monolayer is less stable, the asymmetry was near complete with the entire diffracted signal on one side of the direct beam. Significantly higher intensity was detected than at lower surface pressures allowing Bragg reflections below the horizon of the quartz substrate ($-q_z$) to be observed as well. Further, the negative q_z peak appeared at the opposite side as the positive q_z peak and the position of the diffracted peaks switched sides when the sample was rotated 180°. These observations are consistent with long ranged preferential alignment of the acyl chains induced by the dip direction of the LB deposition which, in all cases, was orthogonal to the

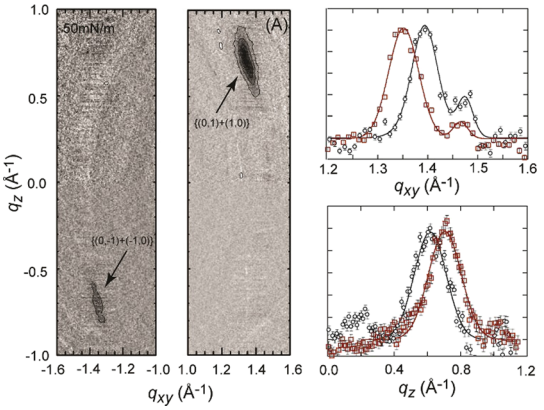

Figure 5. (A) Image plates of GIXD from a DPPC bilayer deposited at 60 mN/m. The absence of reflections above the horizon at $-q_{xy}$ and below the horizon at $+q_{xy}$ indicates long-range preferential alignment of the acyl chains. The reflection at $-q_z$ appears less intense due to attenuation by the quartz substrate. (B) Comparison of Bragg peaks from DPPC bilayers deposited at 50 mN/m (circles) and 60 mN/m (red squares). Solid lines are fits to the Bragg peaks using pseudo Voigt functions. (C) Comparison of Bragg rods from 50 mN/m (circles) and 60 mN/m (red squares) DPPC bilayers. Solid lines are Gaussian fits to the combined {(0,1)+(1,0)} peaks from the bilayers.

X-ray beam direction. Opposite to the trend observed at lower surface pressures, the APM and molecular tilt magnitude in bilayers deposited at 60 mN/m increased significantly compared to 50 mN/m bilayers (Table 1).

DISCUSSION

Lipids adopt a variety of different ordered states which depend on molecular attributes such as headgroup hydration and charge, lipid tail length, and degree of alkyl chain saturation, as well as external factors like temperature and pressure. Here, we focus on the influence of deposition pressure on the structure of gel phase DPPC: a zwitterionic lipid with saturated acyl chains. For monolayers at the air–water interface, steric and VDW interactions between

neighboring head groups and alkyl chains largely determine the phase behavior. In addition to these factors, lipid multilayer structure can also be affected by interactions between the two leaflets and supported bilayer structure affected by both interactions between the inner bilayer leaflet and the substrate and interactions between the two leaflets. With the use of GIXD, the lateral packing of lipids was precisely characterized allowing the more subtle influences on membrane structure in supported bilayers to be compared to monolayer structures. A quantitative comparison of the chain packing between lipid monolayers, bilayers, and multilayers is presented in Figure 6.

As can be clearly seen, the dominant trend for both DPPC monolayers and bilayers is that APM and molecular tilt (θ) of the lipids decrease linearly with increasing surface pressure. The change in APM correlates to the π-A isotherm, which, in the measured range of 20−50 mN/m, is also linear. A corresponding decrease in tilt is also anticipated assuming that the lipid tails maintain a constant cross-sectional area. Predominantly, lipid APM in Langmuir deposited supported bilayers maintains the same pressure dependence as in monolayers. This demonstrates that there is not a significant packing rearrangement of molecules in the bilayer after removing the lateral constraint imposed by the Langmuir trough barrier. Rather than driving to an equilibrium structure, the local molecular packing within a solid supported bilayer is quenched and maintains the structure of the lipid monolayer from which it was deposited. Since this correlation is preserved, bilayers formed by vesicle fusion and subsequent spontaneous self-assembly can be mapped on to these results. In the case of a supported DPPC bilayer formed by vesicle fusion, the local packing most closely matches LB−LS bilayers deposited at 39 ± 3 mN/m. Further systematic studies could determine if vesicle preparation conditions impact the final state of lipid packing in supported lipid bilayers. Previous X-ray diffraction studies of DPPC multilayer structures were also compared to these results.[28,33] Reported values for APM and tilt of lipid multilayer packing was mapped onto the surface pressured dependent trends observed for DPPC monolayers and bilayers. In the case of multilayer stacks, the structural parameters (cross-sectional area, APM, and θ) corresponded closely to a supported bilayer deposited at 26 mN/m. However, the uncertainty in the reported APM prevents making a precise correlation between lipid packing in supported bilayers and multilayer stacks. On the other hand, unoriented DPPC multilayers exhibited a structure intermediate between the monolayer and bilayer trends and were best approximated by a 17 mN/m monolayer. Regardless of

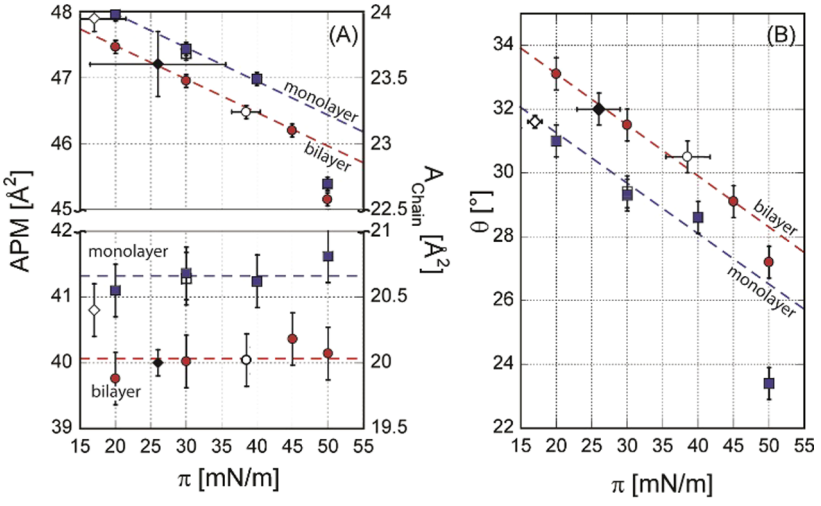

Figure 6. Comparisons of lipid area per molecule (APM), acyl chain cross-sectional area (A_{Chain}), and tilt magnitude in DPPC monolayers, bilayers, and multilayers. Dashed lines are visual guides to the surface pressure dependence for both monolayers and bilayers. For comparison, the APM and tilt obtained from wide-angle X-ray scattering from unoriented DPPC multilayers (open diamond) and oriented multilayer stacks (black diamond) are displayed at the surface pressure that best matches the monolayer or bilayer structure. (A, top) Monolayer APM (blue filled squares) and bilayer APM (red filled circles) are shown as a function of surface pressure. Dashed lines are visual guides to the surface pressure dependence for both monolayers and bilayers. The APM of a solid supported monolayer deposited at 30 mN/m (open square) is shown to be consistent with a 30 mN/m monolayer at the air−water interface. The APM of a DPPC bilayer formed by vesicle fusion (open circle) was found to be consistent with a 38.5 ± 3 mN/m bilayer.[28,33] (A, bottom) Cross-sectional areas of the acyl chains in monolayers at the air−water interface were consistently larger than in supported bilayers. The cross-sectional area of a 30 mN/m monolayer deposited on quartz was roughly equivalent to a monolayer with the same surface pressure at the air−water interface. While oriented multilayer stacks exhibited a cross section consistent with supported bilayers, the lipid cross section in unoriented DPPC multilayers was intermediate between monolayers and bilayers. No significant trends in the cross-sectional area of the acyl chains as a function of surface pressure were observed. (B) The tilt magnitude of lipids in monolayers at the air−water interface (blue, filled squares) and in supported bilayers (filled circles) are shown as a function of surface pressure. For a 30 mN/m monolayer, molecular tilt in a solid supported monolayer (open square) is comparable to a monolayer at the air−water interface. As in the case of APM, the lipid tilt magnitude in DPPC bilayers formed by vesicle fusion (open circle) was consistent with a 38.5 ± 3 mN/m bilayer.

these distinctions, in both cases, the lipid packing within DPPC multilayers corresponded to surface pressures below 30 mN/m, significantly lower than that corresponding to the self-organized vesicle fusion supported bilayer.

Although lipid monolayers and bilayers follow the same overall trends with surface or deposition pressure, the lipid APM was consistently smaller and the molecular tilt consistently larger in supported bilayers than in the monolayers from which they were deposited. What is the origin of these differences: is it interactions with the substrate or leaflet−leaflet interactions? Analyses of the Bragg rods clearly demonstrate that lipids in opposing leaflets are coupled at a molecular level and that this coupling occurs over the full range of surface pressures studied and for bilayers formed by vesicle fusion. No signature of the fwhm associated with uncoupled lipids is observed. Thus, the majority of the lipid tails in the membrane leaflets are in positional and orientational registry. Since the two leaflets of LB deposited bilayers are deposited independently, to obtain molecular coupling, the lipids must self-organize with the inner leaflet serving as a template for the ordering of the outer leaflet. These observations of molecular coupling and templating between the two leaflets are consistent with previous studies of DPPC supported bilayers and multilayers, as well as our results of orientation order dependent on the deposition direction relative to the substrate at high surface pressure (Figure 5).[33,34] In contrast, the interaction between the inner leaflet and the substrate appears to have less of an impact on lipid packing. DPPC monolayers studied at the air−water interface and monolayers deposited onto a solid substrate exhibit similar structures with approximately equivalent APM and molecular tilts. While interactions with the substrate inhibit out-of-plane membrane fluctuations and may thereby facilitate coupling, these results indicate that it is primarily leaflet−leaflet interactions that cause the differences in structure and lipid packing between gel phase DPPC bilayers and monolayers. This suggests that the favorable energy associated with molecular coupling, presumably due to increased VDW contact of the methyl groups at the chain ends, outweighs the loss of entropy caused by restricting the accessible chain orientations and rotations. Several mechanisms have been proposed to describe the coupling of lipid domains across bilayer leaflets ranging from lipid tail interdigitation to chemical potential differences induced by cholesterol flip-flop.[35] Our results show that over a wide range of deposition pressures methyl−methyl VDW interactions are sufficient to induce molecular level coupling across leaflets. Although this mechanism is demonstrated for a model gel phase phospholipid, in principle, methyl−methyl interactions, even between unsaturated lipids, may generally serve to stabilize bilayer organization and play an important role in the correlation of functional microdomains across leaflets as well as impacting membrane curvature and morphology.[36,37]

Typically, a decrease in lipid APM is associated with a concomitant decrease in tilt such that the cross-sectional area of the acyl chains, A_{CS} = (APM/2) cos θ, is conserved. However, the difference in lipid packing between DPPC bilayers and monolayers is inconsistent with a constant acyl chain cross section. For all surface pressures, lipid tail cross sections in bilayers were similar to values reported for oriented multilayer stacks and approximately 0.5 Å^2 less than in monolayers. A possible explanation for the smaller cross section is that lipid chains in bilayers possess less rotational freedom along their long axes. For chains to be able to rotate freely, a distance equal to the longest lateral dimension that passes through the axis of rotation must be maintained between neighboring molecules.[26] A restriction of the chain's rotational freedom would reduce its effective cross section and allow for simultaneously smaller APM and larger molecular tilts. To test this hypothesis, free rotator and nonfree rotator descriptions of chain packing were applied to model Bragg rod intensities. While freely rotating chains fit the monolayer data, only models with rotational ordering of the acyl chains reproduced the GIXD from bilayers. This is consistent with X-ray diffraction and FTIR measurements indicating restricted rotational order of hydrocarbon chains in DPPC multilayers.[29,38] Since restricted rotational order was observed both for bilayers formed by LB−LS deposition and vesicle fusion, this property cannot be attributed to the LB deposition process. Further, diffraction from a solid supported monolayer was consistent with freely rotating chains indicating that substrate interactions do not play a dominant role in restricting chain rotation. On the other hand, rotational order of the lipid chains has not been reported based on DPPC multilayer diffraction results. While diffraction from lipid stacks commonly exhibits features in apparent violation of the multiplicity rule, they are generally attributed to artifacts resulting from attenuation of the scattered intensity by the substrate.[34,39] These artifacts, which are not relevant to the GIXD geometry where monolayer measurements routinely satisfy the multiplicity rule, make quantitative comparison of the relative peak intensities from multilayers difficult. In another case, the apparent violation of the multiplicity rule in DPPC multilayers was quantitatively addressed and attributed to contributions from diffuse scattering.[28] Still, the experimental evidence appears contradictory: the lack of rotational order in multilayers suggests that its presence in supported bilayers is due to substrate interactions while the fact that a free rotator model can be applied to describe a supported monolayer suggests substrate interactions are not responsible. Assuming that multilayer diffraction does

not violate the multiplicity rule, a possible explanation is that a combination of substrate interactions and cross-leaflet coupling is required to restrict the rotational order of the acyl chains. This interpretation is supported by structural differences observed between DPPC monolayers at the air−water interface and on solid supports. Although the supported monolayer did not exhibit rotational ordering of the acyl chains, a greater length of the hydrocarbon scattered in registry presumably due to substrate interactions and the lack of capillary waves on a solid support. The enhanced ordering in supported monolayers may serve to promote stronger lateral interactions and restricted chain orientation in supported bilayers. Alternatively, the opposing results may stem from fundamental differences in the self-organization of lipid multilayers and supported lipid bilayers deposited at higher surface pressures. In this work, we show that the molecular packing in lipid multilayers was found to be consistent with supported bilayers deposited significantly below 30 mN/m and that the molecules in multilayers are not as laterally condensed as bilayers deposited at higher surface pressure. Further, rotational ordering of the acyl chains depends on bilayer deposition pressure with restricted orientations becoming significantly more prominent at 30 mN/m and above. Since DPPC multilayer structure corresponds more closely to supported bilayers deposited at low surface pressure, indications for rotational ordering in the diffraction pattern would be less pronounced and may be difficult to obtain. Even if the specific mechanism cannot be unambiguously identified, these findings suggest that in DPPC bilayers, particularly at high deposition pressures, the VDW interactions between methyl groups that stabilize cross-leaflet coupling restrict the rotational freedom of the acyl chains. Through constraints imposed by the glycerol backbone, the hindered rotational freedom of the acyl chains may further propagate to restrict the orientation of the phosphocholine head groups. Consistent with high resolution AFM images of supported DPPC bilayers, headgroup ordering induced by restricted rotational freedom of the lipid tails may have implications on biological processes ranging from protein recognition, to signaling and trafficking.[40]

Finally, preferential alignment of lipid tilt direction over macroscopic length scales was observed in bilayers deposited at high surface pressures. Tilts were aligned perpendicular to the LB dip direction and persisted across the entire surface of the sample (5 cm^2). Presumably, the deposition process aligned the molecules and maintenance of the long ranged order relied on a sufficiently high deposition pressure, which prevented molecular rearrangement post deposition. This order may have been subsequently locked in through the coupling between bilayer leaflets. However, it is interesting to note that long ranged ordering was only observed at 50 mN/m and above, the regime where the π-A isotherm of the monolayer exhibited instability. We hypothesize that a stiff monolayer is needed to obtain long-range preferential alignment and creating this long-range order comes at the expense of maintaining local packing. Potentially, such control of supported lipid bilayer structure over macroscopic length scales may be exploited by biosensors sensitive to perturbations in lipid tail orientation.[41]

CONCLUSIONS

In this work, lipid order within gel phase DPPC monolayers and supported membranes was compared as a function of the monolayer surface pressure and bilayer deposition pressure. To a first approximation, the in-plane lipid packing within a bilayer deposited by LB−LS is quenched and maintains the same structure as the lipid monolayer from which it was deposited. The ability to control local packing of lipids *via* deposition conditions and maintenance of a quenched structure can potentially be exploited to engineer biosensors. For example, lipid molecular tilt within bilayer based biosensors can be finely tuned to minimize hydrophobic mismatch with targeted membrane proteins. Beyond the general similarity in monolayer and bilayer structure, differences in lipid packing caused by leaflet−leaflet interactions in the bilayer were observed. Lipids in opposing leaflets were invariably coupled maintaining positional and orientational registry across the bilayer. As a result of leaflet−leaflet interactions, lipid bilayers exhibited a slightly smaller area per molecule and larger molecular tilt than their monolayer counterparts at equivalent surface pressure. At higher deposited surface pressure, VDW interactions between the methyl groups that serve to stabilize cross-leaflet coupling also restricted the rotational freedom of the acyl chains in the bilayer. Such findings have not been previously reported based on DPPC multilayer diffraction suggesting that either a combination of leaflet−leaflet interactions and substrate interactions are responsible or that the lateral condensation of molecules in the multilayers is insufficient to significantly restrict acyl chain rotations. Evidence for these interactions provides insight into the mechanism involved in domain coupling and the formation and stabilization of lipid rafts.

MATERIALS AND METHODS

1,2-Dipalmitoyl-*sn*-glycero-3-phosphocholine (DPPC) (T_M 41 °C) was purchased from Avanti Polar Lipids, Inc. (Alabaster, AL). Water was purified with a Milli-Q Gradient water purification system, with a resistivity of >18 MΩ·cm. Single crystal quartz with $\lambda/10$ flatness and 2−3 Å rms roughness was purchased

from Mark Optics (Santa Ana, CA).The pressure−area isotherm (Nima, Coventry, U.K.) of DPPC at room temperature (21 ± 2 °C) is shown in Figure 1A. Monolayers at the air−water interface were studied at the pressures indicated by open arrows on the isotherm. Supported lipid bilayers were prepared by Langmuir−Blodgett (LB)/Langmuir Schaeffer (LS) deposition at the pressures indicated by the solid arrows. For supported bilayers, substrates were solvent cleaned and UV-ozone treated for at least 30 min prior to use. The inner leaflet was deposited by raising the substrates through a compressed DPPC monolayer at the air−water interface at a speed of 1 mm/min (transfer ratio of 1.00 ± 0.05). Subsequently, the substrate surface was aligned parallel to the water interface and the outer DPPC leaflet was deposited at a faster deposition rate of ∼10 mm/min to prevent desorption of the inner leaflet at the air−water interface. Parallelism of the substrate to the interface was critical for ensuring a high transfer of the outer layer. For vesicle fusion formation of supported membranes, a 0.5 mg/mL lipid water solution was probe tip sonicated (Biologics, Manassas, VA) for 1 min and incubated with a clean substrate for 1 h. The sample was then rinsed thoroughly with Milli-Q water to remove unfused vesicles and used without further filtration or centrifugation. All sample preparation was prepared at room temperature (21 ± 2 °C).

X-ray reflectivity (XR) and GIXD are particularly well suited to the study of lipid membranes at interfaces.[42−44] While XR measurements are sensitive to the average electron density distribution normal to the interface, GIXD yields precise in-plane packing properties and, in the case of lipid acyl chains, information on molecular tilt and orientation. Here, XR was used to confirm the formation of high coverage supported DPPC bilayers prior to using GIXD to characterize molecular ordering within the membrane. Monolayer measurements were carried out at the air−water interface on the BW1 beamline at HASYLAB (Hamburg) at a wavelength of λ = 1.304 Å and at the solid-air interface on the I07 beamline at Diamond Light Source (Harwell) at λ = 0.992 Å. Bilayer measurements were carried out at beamline 6-ID at the Advanced Photon Source (Argonne National Laboratory) at λ = 0.545 Å, which enabled measurements through a 1 cm thick water layer. Monolayer measurements were performed at 24 ± 1 °C and bilayer measurements were performed at 25 ± 2 °C. Over these temperature ranges, DPPC Bragg peak position change by less than 0.5%.[45] The formation of DPPC bilayers by Langmuir−Blodgett deposition and vesicle fusion at the SiO_2−water interface was verified by XR. Reflected intensities were measured up to q_z = 0.8 Å^{-1} and modeled to obtain electron density distributions using the Parratt formalism.[46] In all cases, the reflectivity of the bilayers was consistent with that of well packed DPPC membranes with a headgroup to headgroup spacing of 44.0 Å ± 1.0.[7,31] No significant trend or difference was observed in the average electron density distribution of the bilayers as a function of deposition pressure.

Conflict of Interest: The authors declare no competing financial interest.

Acknowledgment. This work was supported by NSF Chemistry Division through grant CHE-0957868. We thank E. Groves for assistance with Langmuir−Blodgett measurements and gratefully acknowledge beamtime at HASYLAB at DESY, Hamburg, Germany, the Diamond Light Source, Oxfordshire, United Kingdom, and the Advanced Photon Source, Argonne National Laboratory, Chicago, IL. Use of the Advanced Photon Source is supported by the Office of Basic Energy Sciences of the U.S. Department of Energy under Contract No. W-31-109-Eng-38.

REFERENCES AND NOTES

1. Sackmann, E. Supported Membranes: Scientific and Practical Applications. *Science* **1996**, *271*, 43–48.
2. Tanaka, M.; Sackmann, E. Supported Membranes as Biofunctional Interfaces and Smart Biosensor Platforms. *Phys. Status Solidi A* **2006**, *203*, 3452–3462.
3. Castellana, E. T.; Cremer, P. S. Solid Supported Lipid Bilayers: From Biophysical Studies to Sensor Design. *Surf. Sci. Rep.* **2006**, *61*, 429–444.
4. Web of Science. **2013**.
5. Tamm, L. K.; Mcconnell, H. M. Supported Phospholipid-Bilayers. *Biophys. J.* **1985**, *47*, 105–113.
6. Gozen, I.; Jesorka, A. Instrumental Methods To Characterize Molecular Phospholipid Films on Solid Supports. *Anal. Chem.* **2012**, *84*, 822–838.
7. Nagle, J. F.; Tristram-Nagle, S. Structure of Llipid Bilayers. *Biochim. Biophys. Acta, Rev. Biomembr.* **2000**, *1469*, 159–195.
8. Kucerka, N.; Nieh, M. P.; Pencer, J.; Harroun, T.; Katsaras, J. The Study of Liposomes, Llamellae and Membranes Using Neutrons and X-rays. *Curr. Opin. Colloid Interface Sci.* **2007**, *12*, 17–22.
9. Daillant, J.; Bellet-Amalric, E.; Braslau, A.; Charitat, T.; Fragneto, G.; Graner, F.; Mora, S.; Rieutord, F.; Stidder, B. Structure and Fluctuations of a Single Floating Lipid Bilayer. *Proc. Natl. Acad. Sci. U.S.A.* **2005**, *102*, 11639–11644.
10. Salditt, T. Thermal Fluctuations and Stability of Solid-Supported Lipid Membranes. *J. Phys.: Condens. Matter* **2005**, *17*, R287–R314.
11. Fragneto, G. Neutrons and Model Membranes. *Eur. Phys. J.: Spec. Top.* **2012**, *213*, 327–342.
12. Pabst, G.; Kucerka, N.; Nieh, M. P.; Rheinstadter, M. C.; Katsaras, J. Applications of Neutron and X-ray Scattering to the Study of Biologically Relevant Model Membranes. *Chem. Phys. Lipids* **2010**, *163*, 460–479.
13. Kucerka, N.; Nagle, J. F.; Sachs, J. N.; Feller, S. E.; Pencer, J.; Jackson, A.; Katsaras, J. Lipid Bilayer Structure Determined by the Simultaneous Analysis of Neutron and X-ray Scattering Data. *Biophys. J.* **2008**, *95*, 2356–2367.
14. Levine, Y. K.; Wilkins, M. H. F. Structure of Oriented Lipid Bilayers. *Nat. (London) New Biol.* **1971**, *230*, 69–&.
15. Levine, Y. K. Physical Studies of Membrane Structure. *Prog. Biophys. Mol. Biol.* **1972**, *24*, 1–74.
16. Tardieu, A.; Luzzati, V.; Reman, F. C. Structure and Polymorphism of Hydrocarbon Chains of Lipids—Study of Lecithin-Water Phases. *J. Mol. Biol.* **1973**, *75*, 711–&.
17. Schalke, M.; Losche, M. Structural Models of Lipid Surface Monolayers from X-ray and Neutron Reflectivity Measurements. *Adv. Colloid Interface Sci.* **2000**, *88*, 243–274.
18. Alsnielsen, J.; Jacquemain, D.; Kjaer, K.; Leveiller, F.; Lahav, M.; Leiserowitz, L. Principles and Applications of Grazing-Incidence X-Ray and Neutron-Scattering from Ordered Molecular Monolayers at the Air-Water-Interface. *Phys. Rep.* **1994**, *246*, 252–313.
19. Kaganer, V. M.; Mohwald, H.; Dutta, P. Structure and Phase Transitions in Langmuir Monolayers. *Rev. Mod. Phys.* **1999**, *71*, 779–819.
20. Koenig, B. W.; Kruger, S.; Orts, W. J.; Majkrzak, C. F.; Berk, N. F.; Silverton, J. V.; Gawrisch, K. Neutron Reflectivity and Atomic Force Microscopy Studies of a Lipid Bilayer in Water Adsorbed to the Surface of a Silicon Single Crystal. *Langmuir* **1996**, *12*, 1343–1350.
21. Fragneto-Cusani, G. Neutron Reflectivity at the Solid/Liquid Interface: Examples of Applications in Biophysics. *J. Phys.: Condens. Matter* **2001**, *13*, 4973–4989.
22. Miller, C. E.; Majewski, J.; Gog, T.; Kuhl, T. L., Characterization of Biological Thin Films at the Solid-Liquid Interface by X-ray Reflectivity. *Phys. Rev. Lett.* **2005**, *94*.
23. Novakova, E.; Giewekemeyer, K.; Salditt, T., Structure of Two-Component Lipid Membranes on Solid Support: An X-ray Reflectivity Study. *Phys. Rev. E* **2006**, *74*.
24. Miller, C. E.; Majewski, J.; Watkins, E. B.; Mulder, D. J.; Gog, T.; Kuhl, T. L., Probing the Local Order of Single Phospholipid Membranes Using Grazing Incidence X-ray Diffraction. *Phys. Rev. Lett.* **2008**, *100*.
25. Kenn, R. M.; Kjaer, K.; Mohwald, H. Non-Rotator Phases in Phospholipid Monolayers? *Colloids Surf., A* **1996**, *117*, 171–181.
26. Sirota, E. B. Remarks Concerning the Relation Between Rotator Phases of Bulk n-Alkanes and those of Langmuir Monolayers of Alkyl-Chain Surfactants on Water. *Langmuir* **1997**, *13*, 3849–3859.
27. Kjaer, K. Some Simple Ideas on X-ray Reflection and Grazing-Incidence Diffration from Thin Surfactant Films. *Physica B* **1994**, *198*, 100–109.

28. Sun, W. J.; Suter, R. M.; Knewtson, M. A.; Worthington, C. R.; Tristramnagle, S.; Zhang, R.; Nagle, J. F. Order and Disorder in Fully Hydrated Unoriented Bilayers of Gel Phase Dipalmitoylphosphatidylcholine. *Phys. Rev. E* **1994**, *49*, 4665–4676.
29. Nagle, J. F. Evidence for Partial Rotational Order in Gel Phase DPPC. *Biophys. J.* **1993**, *64*, 1110–1112.
30. Watkins, E. B.; Miller, C. E.; Majewski, J.; Kuhl, T. L. Membrane Texture Induced by Specific Protein Binding and Receptor Clustering: Active Roles for Lipids in Cellular Function. *Proc Natl. Acad. Sci. U.S.A.* **2011**, *108*, 6975–6980.
31. Watkins, E. B.; Miller, C. E.; Mulder, D. J.; Kuhl, T. L.; Majewski, J., Structure and Orientational Texture of Self-Organizing Lipid Bilayers. *Phys. Rev. Lett.* **2009**, *102*.
32. Dreier, J.; Brewer, J.; Simonsen, A. C. Texture Defects in Lipid Membrane Domains. *Soft Matter* **2012**, *8*, 4894–4904.
33. Tristramnagle, S.; Zhang, R.; Suter, R. M.; Worthington, C. R.; Sun, W. J.; Nagle, J. F. Measurement of Chain Tilt Angle in Fully Hydrated Bilayers of Gel Phase Lecithins. *Biophys. J.* **1993**, *64*, 1097–1109.
34. Katsaras, J.; Yang, D. S. C.; Epand, R. M. Fatty-Acid Chain Tilt Angles and Directions in Dipalmitoyl Phosphatidylcholine Bilayers. *Biophys. J.* **1992**, *63*, 1170–1175.
35. May, S. Trans-Monolayer Coupling of Fluid Domains in Lipid Bilayers. *Soft Matter* **2009**, *5*, 3148–3156.
36. Funkhouser, C. M.; Mayer, M.; Solis, F. J.; Thornton, K. Effects of Interleaflet Coupling on the Morphologies of Multicomponent Lipid Bilayer Membranes. *J. Chem. Phys.* **2013**, *138*, No. 024909.
37. Rangamani, P.; Benjamini, A.; Agrawal, A.; Smit, B.; Steigmann, D. J.; Oster, G. Small Scale Membrane Mechanics. *Biomech. Model. Mechanobiol.* **2013**, 10.1007/s10237-013-0528-6.
38. Le Bihan, T.; Pezolet, M. Study of the Structure and Phase Behavior of Dipalmitoylphosphatidylcholine by Infrared Spectroscopy: Characterization of the Pretransition and Subtransition. *Chem. Phys. Lipids* **1998**, *94*, 13–33.
39. Tristram-Nagle, S.; Liu, Y. F.; Legleiter, J.; Nagle, J. F. Structure of Gel Phase DMPC Determined by X-ray Diffraction. *Biophys. J.* **2002**, *83*, 3324–3335.
40. Sheikh, K. H.; Giordani, C.; Kilpatrick, J. I.; Jarvis, S. P. Direct Submolecular Scale Imaging of Mesoscale Molecular Order in Supported Dipalmitoylphosphatidylcholine Bilayers. *Langmuir* **2011**, *27*, 3749–3753.
41. Bai, Y. Q.; Abbott, N. L. Recent Advances in Colloidal and Interfacial Phenomena Involving Liquid Crystals. *Langmuir* **2011**, *27*, 5719–5738.
42. Spaar, A.; Munster, C.; Salditt, T. Conformation of Peptides in Lipid Membranes Studied by X-ray Grazing Incidence Scattering. *Biophys. J.* **2004**, *87*, 396–407.
43. Wu, G. H.; Majewski, J.; Ege, C.; Kjaer, K.; Weygand, M. J.; Lee, K. Y. C. Interaction between Lipid Monolayers and Poloxamer 188: An X-ray Reflectivity and Diffraction Study. *Biophys. J.* **2005**, *89*, 3159–3173.
44. Miller, C. E.; Busath, D. D.; Strongin, B.; Majewski, J. Integration of Ganglioside GT(1b) Receptor into DPPE and DPPC Phospholipid Monolayers: An X-ray Reflectivity and Grazing-Incidence Diffraction Study. *Biophys. J.* **2008**, *95*, 3278–3286.
45. Sun, W. J.; TristramNagle, S.; Suter, R. M.; Nagle, J. F. Structure of Gel Phase Saturated Lecithin Bilayers: Temperature and Chain Length Dependence. *Biophys. J.* **1996**, *71*, 885–891.
46. Parratt, L. G. Surface Studies of Solids by Total Reflection of X-Rays. *Phys. Rev.* **1954**, *95*, 359–369.